Mapping Nanoscale Absorption of Femtosecond Laser Pulses Using Plasma Explosion Imaging

Daniel D. Hickstein,[†,*] Franklin Dollar,[†] Jennifer L. Ellis,[†] Kyle J. Schnitzenbaumer,[‡] K. Ellen Keister,[†] George M. Petrov,[§] Chengyuan Ding,[†] Brett B. Palm,[∥] Jim A. Gaffney,[⊥] Mark E. Foord,[⊥] Stephen B. Libby,[⊥] Gordana Dukovic,[‡] Jose L. Jimenez,[∥] Henry C. Kapteyn,[†] Margaret M. Murnane,[†] and Wei Xiong[†]

[†]JILA and Department of Physics, University of Colorado, Boulder, Colorado 80309, United States, [‡]Department of Chemistry, University of Colorado, Boulder, Colorado 80309, United States, [§]Plasma Physics Division, Naval Research Lab, Washington, D.C. 20375, United States, [∥]Department of Chemistry, University of Colorado, and CIRES, Boulder, Colorado 80309, United States, and [⊥]Physics Division, Physical and Life Sciences, Lawrence Livermore National Laboratory, Livermore, California 94550, United States

ABSTRACT We make direct observations of localized light absorption in a single nanostructure irradiated by a strong femtosecond laser field, by developing and applying a technique that we refer to as plasma explosion imaging. By imaging the photoion momentum distribution resulting from plasma formation in a laser-irradiated nanostructure, we map the spatial location of the highly localized plasma and thereby image the nanoscale light absorption. Our method probes individual, isolated nanoparticles in vacuum, which allows us to observe how small variations in the composition, shape, and orientation of the nanostructures lead to vastly different light absorption. Here, we study four different nanoparticle samples with overall dimensions of ~100 nm and find that each sample exhibits distinct light absorption mechanisms despite their similar size. Specifically, we observe subwavelength focusing in single NaCl crystals, symmetric absorption in TiO_2 aggregates, surface enhancement in dielectric particles containing a single gold nanoparticle, and interparticle hot spots in dielectric particles containing multiple smaller gold nanoparticles. These observations demonstrate how plasma explosion imaging directly reveals the diverse ways in which nanoparticles respond to strong laser fields, a process that is notoriously challenging to model because of the rapid evolution of materials properties that takes place on the femtosecond time scale as a solid nanostructure is transformed into a dense plasma.

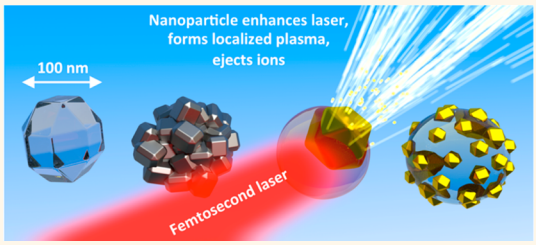

KEYWORDS: plasmonics · local field enhancement · femtosecond lasers · photoion spectroscopy · finite-difference time-domain

The interaction of strong (>10^{13} W/cm^2) laser fields with bulk materials has widespread applications, including precision machining on the submicrometer scale,[1] green synthesis of nanoparticles,[2] and the production of high-energy electrons, ions, and photons.[3] Nanoscale structures can locally enhance a laser field, often by many orders of magnitude,[4] facilitating the generation of strong laser fields that are localized on the nanometer scale, thus paving the way for breakthrough techniques and technologies. For example, gold nanoparticles are being designed to seek out cancerous tumors in the body and, when irradiated with a femtosecond laser, produce shock waves that destroy the tumor with minimal damage to nearby tissues.[5,6] Additionally, several preliminary experiments have demonstrated the ability of laser-irradiated nanostructures to accelerate electrons, suggesting that nanomaterials may enable the fabrication of miniaturized particle accelerators.[7−10] However, transforming these proof-of-principle concepts into practical technologies requires an advanced understanding of how nanostructures respond to light fields that are near the damage threshold.

For laser intensities approaching and exceeding the damage threshold (~3 × 10^{13} W/cm^2 for glass[11] and roughly similar for most other dielectric materials) the interaction of femtosecond laser pulses with bulk materials is a complex process that is extremely challenging to model. The difficulties stem largely from the fact that the laser pulse modifies the optical properties of the material on the femtosecond time

* Address correspondence to danhickstein@gmail.com.

Received for review June 12, 2014 and accepted August 6, 2014.

Published online August 06, 2014
10.1021/nn503199v

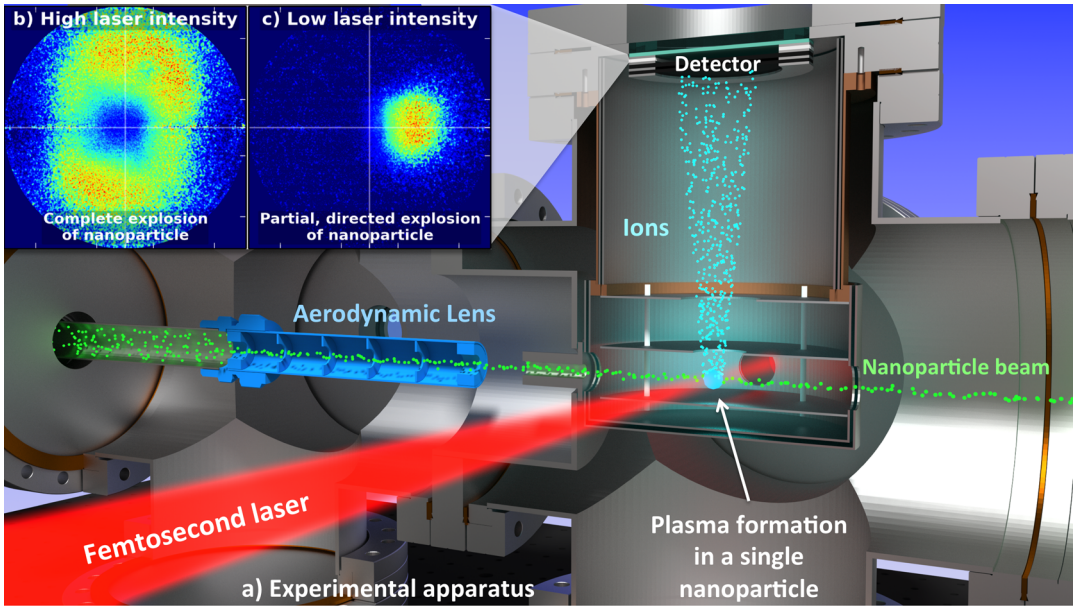

Figure 1. (a) Experimental apparatus for observing plasma explosion imaging in single nanostructures. The nanoparticle aerosol is introduced into the high-vacuum chamber by an aerodynamic lens that produces a collimated beam of nanoparticles. The nanoparticle beam is crossed with a tightly focused 40 fs laser pulse that interacts with a single nanoparticle. (b) When the nanoparticle encounters a region of high laser intensity (>10^{14} W/cm^2), it is completely transformed into a plasma that then ejects ions in all directions. (The apparent lack of ions in the center of the detector is a result of an inhomogeneous detector response.) (c) When the particle encounters a region of low laser intensity, a plasma is formed only in a localized region of the particle, and ions are ejected in a specific direction that depends on the structure, composition, and orientation of the particle. The photoions are collected by a velocity-map-imaging spectrometer and provide information about the localized electric fields in the nanoparticle.

scale,[12] requiring a model that incorporates the properties of the laser field, the solid material, and the newly formed plasma. Materials that exhibit nanoscale structure present a further challenge because features smaller than the wavelength of the light can enhance the electric field on the nanometer scale, and this effect depends strongly on the exact size, shape, and composition of the particle. For example, past work harnessed the ability of nanostructured targets to efficiently absorb laser light to create bright soft X-ray sources,[13] but the detailed mechanisms of this enhancement could not be understood in detail because of the complexity of the interaction. Thus, there is a pressing need for new methods that can provide direct insight into how nanomaterials interact with laser fields.

Direct observation of nanostructures irradiated with intense laser fields presents several experimental hurdles. First, when exposed to intense laser fields, nanostructures are damaged, and thus a fresh sample is required for each laser shot. Second, nanomaterial samples are rarely homogeneous, often varying widely in size, shape, composition, and surface roughness. Even small variations in the morphology of a nanostructure can have a dramatic effect on how the nanostructure responds to incident light fields. When particles of different sizes and shapes are probed simultaneously, these variations are obscured. Finally, the orientation of asymmetric nanoparticles relative to the laser propagation and polarization can dramatically influence how they interact with the light field.

Here we utilize a method that overcomes the experimental hurdles by imaging the localized nanoscale plasma that is created when an isolated nanostructure is irradiated with a short (40 fs), strong (~3×10^{13} W/cm^2) laser pulse. Instead of working with nanoparticles suspended in liquid solution or deposited on a surface, we employ a flowing aerosol of nanoparticles (Figure 1) that provides a fresh nanoparticle for every laser shot, thereby allowing us to use well-established angle-resolved-photoion-spectroscopy techniques.[14−16] Despite probing only a single nanoparticle each laser shot, many particles can be probed each second through the use of a high-repetition-rate femtosecond laser (1 kHz in this study).

A key aspect of our approach is the use of laser intensities slightly *below* the plasma formation threshold of the bulk material, to create a localized nanoplasma only within a specific region of a nanostructure. This method contrasts with previous studies,[10,16] which used laser intensities high enough to field-ionize the entire nanoparticle, creating a uniform plasma throughout the particle. Despite using laser intensities below the plasma formation threshold, we can observe localized plasma formation in the nanoparticles. The formation of plasma at low laser intensities occurs because of nanoscale field enhancements, whereby the nanoparticle itself enhances the laser field in

localized regions. Thus, while the average laser intensity is below the plasma formation threshold, some regions of the nanoparticle can experience light fields higher than threshold, and a plasma will be formed only in these regions of the nanoparticle. The heated plasma is rapidly ejected outward from the surface of the nanoparticle, producing ions with momenta that point to the location of the plasma in the nanoparticle. By observing the momenta of the ejected ions, we can determine the location of the plasma in the nanoparticle. We record a two-dimensional projection of the three-dimensional angular distributions of the ions using an angle-resolved imaging detector. We refer to this technique as plasma explosion imaging and show how it can be used to gain insight into the unusual light-absorbing properties of nanomaterials.

Using this new approach, we observe dramatic differences in how nanoparticles of different compositions and shapes respond to intense laser fields. Specifically, we observe subwavelength focusing in NaCl and symmetrical absorption in aggregates of TiO_2 particles, as well as highly localized light absorption in gold−dielectric hybrid nanostructures. Surprisingly, we find that we can model light absorption in this strong-field regime using the finite-difference time-domain (FDTD) method, which has seen great success in modeling low-intensity-light−nanoparticle interactions. This agreement suggests that many of the useful nanoscale optical effects that exist at low laser intensities (such as subwavelength focusing and plasmonic effects) will extend into the near-damage-threshold regime, where they are expected to begin to breakdown. By demonstrating the nano-optical effects present at laser intensities near and above the material damage threshold, we pave the way for future developments that use the unique ability of nanoparticles to absorb, scatter, and focus light in the regime laser intensities above the damage threshold.

RESULTS AND DISCUSSION

A complete description of the sample preparation and experimental apparatus is found in the Methods section. To perform photoion spectroscopy on isolated nanostructures, we employ an aerodynamic lens,[17−19] which produces a collimated beam of nanoparticles from a nanoparticle aerosol but leaves the carrier gas divergent. A skimmer then allows us to achieve a high-concentration beam of nanoparticles while maintaining high vacuum (1×10^{-6} mbar) in the photoion spectrometer. The particle beam is irradiated with tightly focused, intense ($\sim 3 \times 10^{13}$ W/cm^2), 785 nm, 40 fs laser pulses. Because of the tight focusing of the laser and the narrow width of the particle beam, the volume of the interaction region is only 10^{-7} cm^3 (see Methods). Since the particle density is $\sim 10^5$ particles/cm^3, only one laser shot in ~100 will hit a nanoparticle, and those that do, typically hit only one particle. The photoions produced from the laser-irradiated nanoparticles are collected by a velocity-map-imaging (VMI) photoion spectrometer,[14−16,19−21] which produces images of the ion momentum distribution.

To develop a broad understanding of how nanostructures of different shape and size interact with laser fields near the damage threshold, we prepared a range of nanoparticle aerosols starting with four different aqueous solutions: NaCl, ~5 nm TiO_2 nanoparticles, 50 nm gold nanospheres, and 17 nm gold nanospheres. The nanoparticle aerosols were generated from aqueous solutions using a compressed-gas atomizer, which produces droplets with an average diameter of ~1 μm. Before entering the vacuum chamber, the droplets evaporate to leave single crystals (when using a salt solution) or aggregated nanostructures (when using a colloidal solution) consisting of one or more nanoparticles. The concentration of the material in solution determines the average diameter of the crystals (or the average number of nanospheres per aggregate).

To understand the morphology of the various nanostructures, we performed transmission electron microscopy (TEM) on nonirradiated nanostructures collected at the exact point where they would be probed by the laser. The TEM images (Figure 2) reveal that the nanostructures that emerge from the aerodynamic lens are often quite different from the structures that exist in the solution phase. The NaCl solution produces particles with an average diameter of ~100 nm (Figure 2a). Since crystal faces are clearly visible in many of the particles, we conclude that most of the nanoparticles are single crystals of NaCl, consistent with previous studies of salt aerosols.[22] The TiO_2 particles present as 50−100 nm aggregates of ~5 nm TiO_2 particles (Figure 2b). The aggregates form because many ~5 nm TiO_2 crystals are present in a single droplet. As the droplet evaporates, the nanoparticles clump into larger aggregates.

The morphology of the aerosol particles generated from the aqueous solutions of gold nanospheres is surprising; heterogeneous nanostructures are clearly seen in the TEM images (Figure 2c and d). For the solution of 50 nm gold nanospheres, the aerosol particles typically consist of one 50 nm gold nanosphere embedded near the surface of a ~100 nm sphere of lower density material. The low-density material is polyvinylpyrrolidone (PVP), an organic polymer that is added to the solution by the manufacturer in a similar concentration to that of the nanospheres and serves to keep the nanospheres dispersed in solution.

The solution of 17 nm gold nanospheres also displays a heterogeneous morphology with gold spheres imbedded in PVP (Figure 2d). However, the number concentration of the gold nanospheres is much higher, and the aerosol particles generated from this solution often contain 10 or more gold nanospheres. Thus, while the composition of the 17 and 50 nm gold

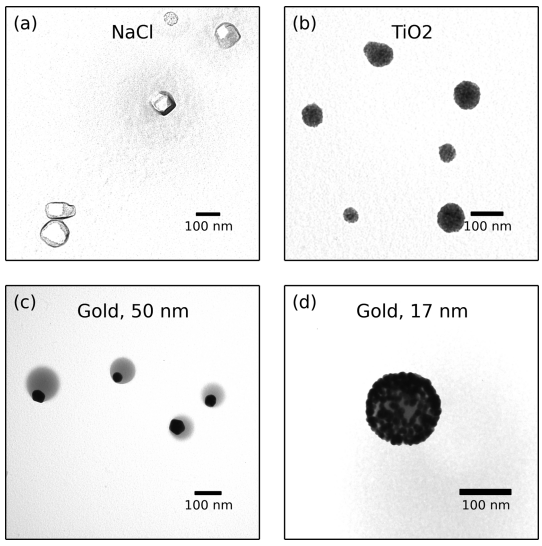

Figure 2. TEM images of nanoparticles collected at the interaction region. (a) The aqueous NaCl solution evaporates to form single crystals. (b) The solution of TiO_2 nanoparticles produces 50−100 nm diameter aggregates of ~5 nm particles. (c) The solution of 50 nm gold nanoparticles produces hybrid nanostructures consisting of a single gold nanoparticle residing near the surface of a sphere of polyvinylpyrrolidone (PVP). (d) The solution of 17 nm gold nanoparticles also generates hybrid gold−PVP nanostructures, but these nanostructures contain numerous 17 nm gold nanospheres.

nanospheres samples is similar in aqueous solution, the aerosol particles display starkly different morphologies. Interestingly, for both the 50 and 17 nm gold nanosphere samples, the gold nanospheres are almost invariably located toward the outside of the PVP nanosphere.

As shown in Figure 1, a collimated beam of nanostructures is introduced into the VMI spectrometer *via* the aerodynamic lens, and individual nanostructures are probed with femtosecond laser pulses. Though the focused laser has a Gaussian intensity profile, the full-width at half-maximum is on the order of 20 μm, which is very large compared to the ~100 nm dimensions of the nanostructures used in this study and means that each particle experiences a nearly homogeneous electric field. When the laser intensity exceeds $\sim 5 \times 10^{13}$ W/cm^2, the laser delivers enough energy to create a plasma in the entire nanoparticle (Figure 1b). In contrast, at intensities near 3×10^{13} W/cm^2, a plasma is formed only in a small region of the particle (Figure 1c). Since it is these "localized plasma" cases that provide information about the local-field enhancement, they are the focus of this work. Creating primarily localized plasmas is achieved by keeping the laser intensity in a range such that only the most intense regions of the laser focus are capable of creating a plasma in a nanoparticle.

The mechanism for plasma formation in solid-density materials irradiated with femtosecond pulses near the damage threshold is typically described as an avalanche ionization process.[23−25] First, a few free electrons are generated through multiphoton or tunnel ionization of the material (for conductors, free electrons already exist in the material). Next, these free electrons are driven by the strong laser field and can reach kinetic energies exceeding the ionization threshold. When an electron impacts an atom, it can remove one or more electrons through electron impact ionization. The newly liberated electrons can then cause more ionization in an avalanche process. Both the initial ionization process and the avalanche ionization process scale exponentially with laser intensity,[26] and, therefore, a small increase in the laser intensity in certain regions of the nanoparticle can have a very large effect on the ionization rate and, in turn, determine if complete breakdown of the material will occur.

Given the field-driven avalanche breakdown mechanism, it is conceivable that any ionization within the nanoparticle would create free electrons, which could then ionize neighboring atoms, initiating rapid ignition over the entire nanostructure. However, the excursion distance of a free electron driven by a 785 nm laser field at an intensity of 5×10^{13} W/cm^2 is only ~1 nm. In addition, we estimate the plasma temperature to be ~5 eV,[16] which does not provide the thermal electrons enough kinetic energy to propagate more than a few nanometers during the laser pulse. Consequently, the free electrons cannot travel to all regions of a ~100 nm nanoparticle during the duration of the laser pulse. Rather, at intensities near the damage threshold, avalanche breakdown stays localized near the region of initial ionization, which is the region that experienced the highest local field. Thus, the physical location of the localized plasma serves as a map of the locally enhanced laser field that caused the avalanche breakdown.

After the laser pulse is over (<0.1 ps), the region of localized plasma rapidly expands on the picosecond time scale, attempting to eject ions in all directions.[16] However, those ions that are launched inward (toward the undamaged material) cannot penetrate the material (because of their low kinetic energy) and do not reach the detector. We observe only ions that are launched away from the undamaged regions of the nanostructure. As a result, we can interpret the angular features in the photoion *momentum* distribution as a direct result of *spatial* location of the localized plasma in the nanostructure. The photoelectrons can provide similar information to the photoions (see Supporting Information, Figure S1), but with somewhat less resolution due to the increased scattering of the electrons compared to the ions. Thus, we choose to focus on the photoions in this study. Using mass spectroscopy (Figure S2), we confirm that the photoions that reach the detector are primarily from the nanoparticles and not from other sources, such as the background gas.

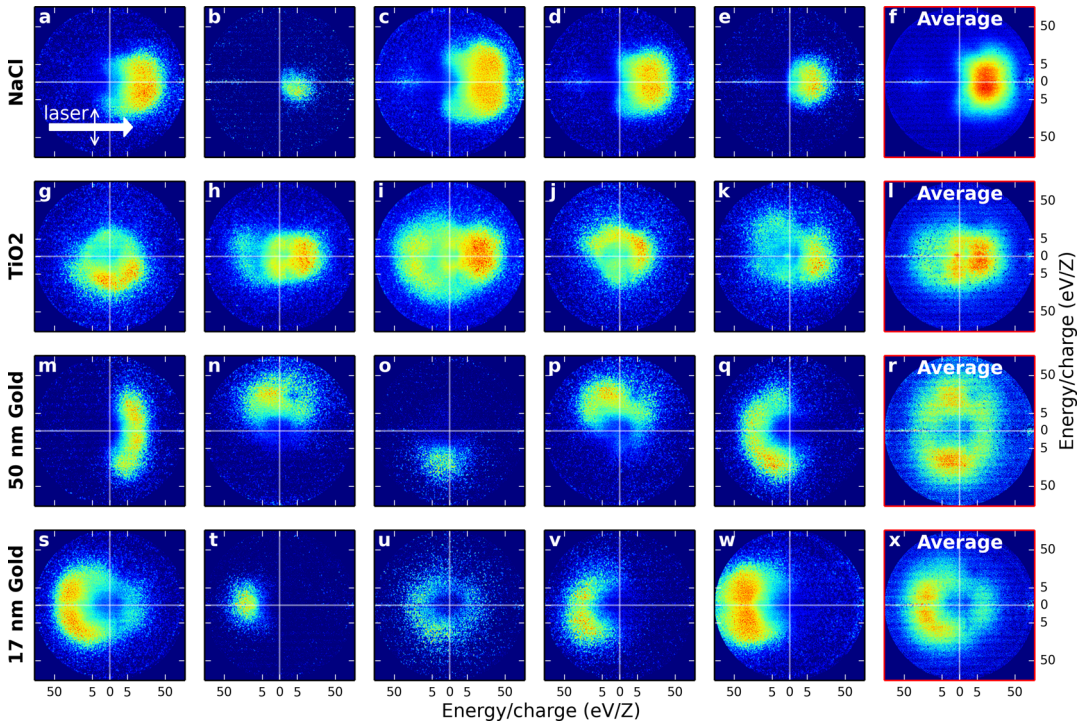

Figure 3. Photoion angular distributions from individual nanostructures show ions ejected in different directions. The laser propagates from left to right and is polarized in the vertical direction, although no polarization dependence is observed in this study. (a–f) The photoions from ~100 nm NaCl crystals are ejected in the laser propagation direction, suggesting a focusing effect. (g–l) The ions from TiO_2 aggregates are typically centered around zero kinetic energy, indicating mostly symmetric plasma formation. (m–r) Photoions from 50 nm gold nanoparticles imbedded in a larger PVP sphere eject ions with directions that depend on the orientation of the nanostructure. (s–x) Photoions from 17 nm gold–PVP nanostructures eject ions in the direction opposite of the laser propagation, indicating absorption of laser energy on the front (illuminated) side of the nanoparticle. The averaged images (f, l, r, x) correspond to 70, 869, 419, and 108 particles, respectively, and reveal general trends, but conceal the diversity of the individual particles, especially in the case of the 50 nm gold sample.

For all of the nanostructure samples investigated, we observe considerable hit-to-hit variations in the photoion angular distributions (Figure 3), reflecting the differences in the shape, composition, and orientation of the particles. Despite the hit-to-hit variations, we can easily spot general trends in the direction of ion ejection in the four samples presented here. These trends are summarized in Figure 3 and confirmed *via* the center-of-mass distributions presented in Figure 4. To understand the physical origin of the localized light absorption in each nanostructure, finite-difference time-domain methods were used to simulate the interaction of 785 nm femtosecond pulses with the nanomaterials (Figure 5 and Methods for details). Figure 6 presents a summary of the different light absorption mechanisms observed in the various nanostructures.

NaCl Crystals: Nanofocusing in Dielectric Nanomaterials. In the case of the ~100 nm NaCl crystals, ion ejection is observed almost exclusively in the forward direction, *i.e.*, the direction of laser propagation (Figures 3a and 4a). This effect is the opposite of what we expect for an opaque macroscopic object, which would absorb light primarily on the illuminated side and eject material back toward the laser. It is also different from what we would expect at laser intensities well above the damage threshold, where the high electron densities would cause the resulting plasma to act like a metal, again absorbing energy on the surface facing the laser. Instead, we observe that a ~100 nm NaCl crystal acts like a lens, focusing the light onto itself and forming a plasma on the back side. Of course, strictly speaking, we cannot apply the term "focusing" in this case, since geometric optics does not describe the interaction of light with objects smaller than the wavelength. However, numerous studies of "photonic nanojets"[27–32] have confirmed the ability of nanoparticles to concentrate visible light on length scales far smaller than the wavelength, a phenomenon referred to as subwavelength focusing.

Indeed, our FDTD simulations confirm the subwavelength focusing of the NaCl particles, revealing a ~10% increase of the light intensity on the back side of the particle compared to the front side (Figure 5a). While this increase is relatively modest compared to the intense lensing observed in micrometer-sized dielectric particles,[29] our experiment is operated in a regime very close to the threshold for plasma formation, and a small increase in intensity can have dramatic effects on the highly nonlinear plasma formation process.

TiO_2 Nanoclusters: Light Interaction with a Particle Ensemble. The overall size of the TiO_2 aggregates is similar to the NaCl crystals (both are ~100 nm). However, in contrast

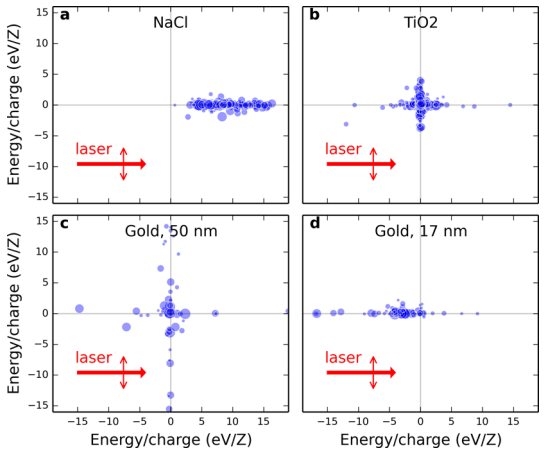

Figure 4. Position of the center of mass of the ion distributions for various nanoparticle samples. The position of each dot indicates the center of mass of the photoion distributions, and larger sizes correspond to higher ion yield. (a) NaCl particles act as lenses, focusing the light onto the back side of the particle and ejecting ions primarily in the laser propagation direction. (b) TiO_2 undergoes plasma formation over the entire particle, generating plasma explosions that are largely symmetric about zero kinetic energy. (c) The 50 nm gold nanosphere samples produce composite nanostructures consisting of gold nanospheres imbedded in a dielectric material. A plasma is preferentially formed in the gold nanosphere that explodes outward, ejecting ions in a direction that depends on the orientation of the nanostructure, but not on the laser polarization or propagation directions. (d) The 17 nm gold nanospheres form aggregate nanostructures consisting of many gold nanospheres that absorb mainly on the illuminated face and eject ions opposite the direction of laser propagation.

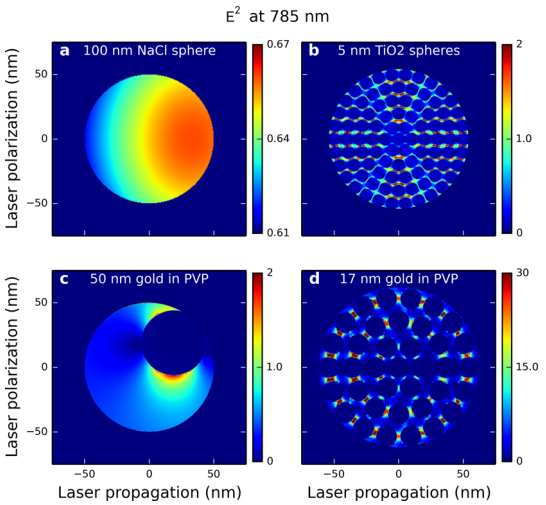

Figure 5. FDTD calculations of the electric field intensity inside the various nanostructures. The laser propagates from left to right, and the color scale is in units of the incident field intensity. Plasma formation is most likely to occur near the regions of highest electric field. (a) In the NaCl particles, the laser field is enhanced by approximately 10% on the side opposite of the light source. (b) In the TiO_2 aggregates, the highest electric field is in the regions between the TiO_2 particles and does not have a preference for the laser polarization or laser propagation directions. (c) For the 50-nm-gold−PVP nanostructures, the electric field is enhanced substantially near the surface of the gold nanoparticle, which likely ignites a localized plasma in the dielectric material. (d) In the structures composed of 17 nm gold nanospheres, the light field is greatly enhanced in hot spots between the nanospheres, and higher fields are seen on the illuminated side of the nanostructure.

to NaCl, the ion ejection from the TiO_2 particles is generally symmetric about zero kinetic energy (Figures 3b and 4b). This effect cannot be explained by a difference in the material properties, because both TiO_2 and NaCl are transparent materials with a band gap larger than the photon energy. Given this similarity, one would expect TiO_2 to exhibit the same subwavelength focusing that takes place in NaCl. The different response can be explained by the fact that the large TiO_2 aggregates are composed of many ~5 nm crystals instead of a single large crystal. This isolation of individual particles prevents the focusing effect that occurs in NaCl single crystals. Accordingly, our FDTD simulations (Figure 5b) reveal considerable enhancement of the electric field on the surface of the 5 nm TiO_2 nanoparticles, but show no preference for the front or back of the 100 nm aggregate. Thus, we see that by simply changing from a single crystal to a similarly sized aggregate of smaller particles, we can completely change the light absorption properties of the material, even at a scale much smaller than the wavelength of the light.

Gold Nanoparticles of 50 nm: Field Enhancement at the Surface. The gold-nanosphere−dielectric nanostructures are of particular interest, because the 50 and 17 nm gold nanoparticle samples are identical in chemical composition but exhibit vastly different properties because of their different morphologies. For 50 nm gold nanostructures, the ion explosions are directional, but the direction is random with respect to the laser (Figure 3c and Figure 4c). Explosions were observed in the direction of laser propagation, in the opposite direction, and in orthogonal directions with equal probability. Thus, the direction of the explosion is not set by the laser, but by the spatial orientation of the nanostructure.

Gold nanoparticles are well known to enhance the electric field at their surface,[27,33−35] and this enhancement likely ignites the plasma formation process in the vicinity of the gold nanosphere. Additionally, being a metal, the gold particles already have conduction band electrons, which are freely driven by the laser and absorb energy through collisions with the ions. Thus, the heating of the gold nanosphere will begin before the laser pulse has reached maximum intensity, in contrast to the PVP, which must be ionized before it can strongly absorb energy from the laser pulse. Both of these effects lead to a strong absorption of laser energy in the immediate vicinity of the gold nanosphere, which leads to a localized plasma formation. This localized plasma creates a directional ion ejection in a direction set by the orientation of the nanostructure. This rationalization is confirmed by the FDTD simulations (Figure 5c), which reveal that the laser field

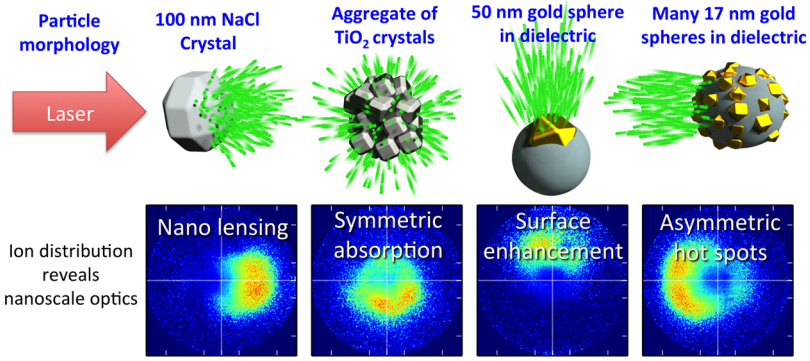

Figure 6. Summary of nanoscale light absorption mechanisms revealed through plasma explosion imaging. While all particles presented here have similar diameters (~100 nm), they absorb light in different ways, form a localized plasma in different locations, and exhibit different characteristic photoion distributions, which indicate the light absorption mechanism for a single isolated nanoparticle.

is greatly enhanced by more than 200% near the surface of the gold nanoparticle.

Gold Nanospheres of 17 nm: Asymmetric Hot Spots. Interestingly, the 17-nm-gold–PVP hybrid nanostructures display completely different behavior than 50 nm gold nanostructures; the ions are ejected primarily in the backward direction (Figures 3d and 4d). The difference stems from the fact that the 50 nm sample produces nanoparticles that contain only one gold nanosphere, while the 17 nm sample produces PVP nanoparticles that contain numerous 17 nm gold spheres. Since the 17 nm spheres are located in close proximity to one another (Figure 2d), the electric field can be enhanced by nearly an order of magnitude in the regions between the gold nanospheres (Figure 5d). It is likely that the plasma formation takes place in the PVP in the electric field hot spots[36] between the gold nanoparticles. The FDTD calculations reveal that these hot spots are most pronounced on the side of the aggregate that faces the laser, suggesting that plasma will preferentially form on this face of the particle. In analogy to geometric optics, it appears that the gold nanoparticles on the illuminated side are blocking the light from reaching the back side of the particle.

Future Directions. In this study we focused on laser intensities near the ablation threshold, and consequently, we were able to successfully simulate the laser ablation process using numerical methods that ignore the changes in the material properties that take place at high laser intensities such as the nonlinear refractive index or the excitation of charge carriers to the conduction band. It is likely that such effects begin to dominate as the laser intensity is increased. Future studies could utilize the plasma explosion imaging method to search for these nonlinear effects at laser intensities well above the plasma formation threshold. Indeed, a close examination of Figure 1b reveals that, while the high-intensity explosion of the nanoparticle ejects ions in all directions, it is not completely homogeneous. Thus, the plasma explosion imaging method can likely provide information about laser–nanoparticle interactions at intensities well above the damage threshold.

SUMMARY

We have demonstrated a new technique called plasma explosion imaging, where we use strong femtosecond laser fields to create a localized plasma within isolated nanoparticles and use the momentum of the ejected ions to infer the location of this plasma within individual nanoparticles. The location of the plasma indicates where the electric fields are enhanced in the particle and provides a map of the nanoscale light absorption at laser intensities near the damage threshold. We apply this novel method to observing subwavelength focusing in NaCl, symmetric plasma formation in TiO_2 clusters, and highly localized plasma formation in gold–dielectric hybrid nanostructures. In the future, this method can be easily extended to more complex nanostructures and higher laser intensities, providing further insight into the interaction of strong laser fields with nanomaterials.

METHODS

Photoion Spectroscopy and Aerosol Generation. To perform velocity-map-imaging spectroscopy on nanostructures (nanoVMI), we generate a nanoparticle aerosol, consisting of isolated nanoparticles suspended in N_2 gas. The aerosol enters a low-vacuum chamber through an aerodynamic lens[17,18] (Aerodyne Research) that collimates the particles into a ~0.5 mm beam, but leaves the carrier gas divergent. The collimated particle beam passes through a 1.5 mm skimmer and enters the photoion spectroscopy chamber, which is maintained at 1×10^{-6} mbar (base pressure 1×10^{-8} mbar). The particles are then irradiated by an intense (~3×10^{13} W/cm^2), 785 nm, 40 fs laser pulse, derived from a Ti:sapphire regenerative amplifier (KMLabs Wyvern HE) operating at 1 kHz.

The laser is focused using a 40 cm lens to reach an approximate diameter of 20 μm, which—considering the width of the particle beam (0.05 cm)—provides an interaction volume of approximately 10^{-7} cm^3. Because the density of the nanoparticles is only ~10^5 particles/cm^3, the hit rate is ~0.01 particle

per laser shot. The photoions originating from the laser-irradiated nanoparticles are imaged by a velocity-map-imaging spectrometer,[14] which projects the expanding ion distribution onto a detector consisting of a microchannel plate (MCP) and phosphor screen. The angular-resolved momentum distribution of the ions is then recorded using a CCD camera (Allied Vision Technologies) operating at ~15 Hz. The exposure time of the camera is adjusted to ensure that each frame consists of only one particle hit.

Materials. We obtained pure NaCl from Sigma-Aldrich and ~5 nm TiO_2 nanoparticles from US Research Nanomaterials. The 50 and 17 nm gold nanospheres were obtained from Nanocomposix. All samples were used as received, except for dilution in ultrapure (>15 MΩ resistivity) water. The liquid samples are converted into an aerosol using a Collison-type compressed-gas atomizer (TSI) backed with 30 psig of N_2 carrier gas.

Transmission Electron Microscopy. To characterize the nanoparticles probed by the laser, we performed TEM on particles collected in the high-vacuum chamber. TEM grids were inserted into the chamber using a linear actuator passing through an airlock. The TEM grids were positioned at the exact position where the laser crosses that particle beam, and high-velocity particles were collected on the grids for 10 to 30 s. TEM images were obtained using a Phillips CM100 transmission electron microscope.

FDTD Simulations. To understand the results obtained with photoion spectroscopy, we employed finite-difference time-domain simulations implemented in the FDTD Solutions[37] software package (Lumerical, Solutions Inc.) to simulate the interaction of the laser field with the nanoparticles. We simulated the interaction of 40 fs pulses with a central wavelength of 785 nm with several different structures that are representative of the actual geometry of our nanoparticles. The TiO_2 particles were simulated as a collection of six layers of 5 nm dielectric spheres with n = 2.523 (the refractive index of TiO_2 at 785 nm[38]). The NaCl nanocystals were simulated as 100 nm diameter dielectric spheres with n = 1.536 (the refractive index of NaCl[39] at 785 nm). The gold/PVP heterostructures were simulated as 50 or 17 nm gold spheres imbedded in a dielectric sphere with n = 1.4 (the approximate index of PVP[40]). The refractive index of gold is given by the Palik[41] model.

Conflict of Interest: The authors declare no competing financial interest.

Supporting Information Available: In the Supporting Information, we present a photoelectron distribution from single nanoparticles (Figure S1) and a mass spectrum from a single nanoparticle (Figure S2). This material is available free of charge *via* the Internet at http://pubs.acs.org.

Acknowledgment. We thank T. Dimiduk and J. Fung for assistance with preliminary Mie theory calculations and acknowledge insightful conversations with A. Grubisic. We also thank A. Saunders at Nanocomposix for advice regarding gold nanoparticles and J. Phillips for assistance preparing the manuscript. D.D.H., W.X., F.D., C.D., K.E.K., J.L.E., M.M.M., and H.C.K. acknowledge support from the DOE Office of Fusion Energy Sciences DE-SC0008803 and equipment support from an NSSEFF Fellowship. B.B.P. and J.L.J. thank DOE DE-SC0011105 and NOAA NA13OAR4310063 for support. S.B.L., M.E.F, and J.A.G. acknowledge support from the DOE Office of Fusion Energy, HED Laboratory Plasmas program under grant AT5015033. Lawrence Livermore National Laboratory is operated by Lawrence Livermore National Security, LLC, for the U.S. Department of Energy, National Nuclear Security Administration, under contract DE-AC52-07NA27344. G.M.P. acknowledges support by the Naval Research Laboratory 6.1 Base Program. K.J.S. and G.D. acknowledge support from the Air Force Office of Scientific Research under AFOSR award no. FA9550-12-1-0137. Dr. Wei Xiong is presently affiliated with the Department of Chemistry and Biochemistry, University of California San Diego, La Jolla, California 92093, United States.

REFERENCES AND NOTES

1. Pronko, P. P.; Dutta, S. K.; Squier, J.; Rudd, J. V. Machining of Sub-micron Holes Using a Femtosecond Laser at 800 nm. *Opt. Commun.* **1995**, *114*, 106–110.
2. Amendola, V.; Meneghetti, M. Laser Ablation Synthesis in Solution and Size Manipulation of Noble Metal Nanoparticles. *Phys. Chem. Chem. Phys.* **2009**, *11*, 3805–3821.
3. Hatchett, S. P.; Brown, C. G.; Cowan, T. E.; Henry, E. A.; Johnson, J. S.; Key, M. H.; Koch, J. A.; Langdon, A. B.; Lasinski, B. F.; Lee, R. W.; *et al*. Electron, Photon, and Ion Beams from the Relativistic Interaction of Petawatt Laser Pulses with Solid Targets. *Phys. Plasmas* **2000**, *7*, 2076–2082.
4. Le Ru, E. C.; Blackie, E.; Meyer, M.; Etchegoin, P. G. Surface Enhanced Raman Scattering Enhancement Factors: A Comprehensive Study. *J. Phys. Chem. C* **2007**, 13794–13803.
5. Pustovalov, V. K.; Smetannikov, A. S.; Zharov, V. P. Photothermal and Accompanied Phenomena of Selective Nanophotothermolysis with Gold Nanoparticles and Laser Pulses. *Laser Phys. Lett.* **2008**, *5*, 775–792.
6. Lachaine, R.; Boulais, É.; Meunier, M. From Thermo- to Plasma-Mediated Ultrafast Laser-Induced Plasmonic Nanobubbles. *ACS Photonics* **2014**, *1*, 331–336.
7. Peralta, E. A.; Soong, K.; England, R. J.; Colby, E. R.; Wu, Z.; Montazeri, B.; McGuinness, C.; McNeur, J.; Leedle, K. J.; Walz, D.; *et al*. Demonstration of Electron Acceleration in a Laser-Driven Dielectric Microstructure. *Nature* **2013**, *503*, 91–94.
8. Kaplan, A. E.; Dubetsky, B. Y.; Shkolnikov, P. L. Shock Shells in Coulomb Explosions of Nanoclusters. *Phys. Rev. Lett.* **2003**, *91*, 143401.
9. Peano, F.; Fonseca, R. A.; Silva, L. O. Dynamics and Control of Shock Shells in the Coulomb Explosion of Very Large Deuterium Clusters. *Phys. Rev. Lett.* **2005**, *94*, 033401.
10. Ditmire, T.; Tisch, J. W. G.; Springate, E.; Mason, M. B.; Hay, N.; Marangos, J. P.; Hutchinson, M. H. R. High Energy Ion Explosion of Atomic Clusters: Transition from Molecular to Plasma Behavior. *Phys. Rev. Lett.* **1997**, *78*, 14–17.
11. Schaffer, C. B.; Brodeur, A.; García, J. F.; Mazur, E. Micromachining Bulk Glass by Use of Femtosecond Laser Pulses with Nanojoule Energy. *Opt. Lett.* **2001**, *26*, 93–95.
12. Durach, M.; Rusina, A.; Kling, M. F.; Stockman, M. I. Predicted Ultrafast Dynamic Metallization of Dielectric Nanofilms by Strong Single-Cycle Optical Fields. *Phys. Rev. Lett.* **2011**, *107*, 086602.
13. Murnane, M. M.; Kapteyn, H. C.; Gordon, S. P.; Bokor, J.; Glytsis, E. N.; Falcone, R. W. Efficient Coupling of High-Intensity Subpicosecond Laser Pulses into Solids. *Appl. Phys. Lett.* **1993**, *62*, 1068–1070.
14. Eppink, A. T. J. B.; Parker, D. H. Velocity Map Imaging of Ions and Electrons Using Electrostatic Lenses: Application in Photoelectron and Photofragment Ion Imaging of Molecular Oxygen. *Rev. Sci. Instrum.* **1997**, *68*, 3477–3484.
15. Hickstein, D. D.; Ranitovic, P.; Witte, S.; Tong, X.-M.; Huismans, Y.; Arpin, P.; Zhou, X.; Keister, K.; Hogle, C.; Zhang, B.; *et al*. Direct Visualization of Laser-Driven Electron Multiple Scattering and Tunneling Distance in Strong-Field Ionization. *Phys. Rev. Lett.* **2012**, *109*, 073004.
16. Hickstein, D. D.; Dollar, F.; Gaffney, J. A.; Foord, M. E.; Petrov, G. M.; Palm, B. B.; Keister, K. E.; Ellis, J. L.; Ding, C.; Libby, S. B.; *et al*. Observation and Control of Shock Waves in Individual Nanoplasmas. *Phys. Rev. Lett.* **2014**, *112*, 115004.
17. Zhang, X.; Smith, K. a.; Worsnop, D. R.; Jimenez, J. L.; Jayne, J. T.; Kolb, C. E.; Morris, J.; Davidovits, P. Numerical Characterization of Particle Beam Collimation: Part II. Integrated Aerodynamic-Lens–Nozzle System. *Aerosol Sci. Technol.* **2004**, *38*, 619–638.
18. Liu, P. S. K.; Deng, R.; Smith, K. A.; Williams, L. R.; Jayne, J. T.; Canagaratna, M. R.; Moore, K.; Onasch, T. B.; Worsnop, D. R.; Deshler, T. Transmission Efficiency of an Aerodynamic Focusing Lens System: Comparison of Model Calculations and Laboratory Measurements for the Aerodyne Aerosol Mass Spectrometer. *Aerosol Sci. Technol.* **2007**, *41*, 721–733.
19. Wilson, K. R.; Zou, S.; Shu, J.; Ru, E.; Leone, S. R.; Schatz, G. C.; Ahmed, M. Size-Dependent Angular Distributions of Low-Energy Photoelectrons Emitted from NaCl Nanoparticles. *Nano Lett.* **2007**, *7*, 2014–2019.
20. Durach, M.; Rusina, A.; Kling, M. F.; Stockman, M. I. Predicted Ultrafast Dynamic Metallization of Dielectric Nanofilms by Strong Single-Cycle Optical Fields. *Phys. Rev. Lett.* **2011**, *107*, 086602.

21. Xiong, W.; Hickstein, D. D.; Schnitzenbaumer, K. J.; Ellis, J. L.; Palm, B. B.; Keister, K. E.; Ding, C.; Miaja-Avila, L.; Dukovic, G.; Jimenez, J. L.; *et al*. Photoelectron Spectroscopy of CdSe Nanocrystals in the Gas Phase: A Direct Measure of the Evanescent Electron Wave Function of Quantum Dots. *Nano Lett.* **2013**, *13*, 2924–2930.
22. Zelenyuk, A.; Cai, Y.; Imre, D. From Agglomerates of Spheres to Irregularly Shaped Particles: Determination of Dynamic Shape Factors from Measurements of Mobility and Vacuum Aerodynamic Diameters. *Aerosol Sci. Technol.* **2006**, *40*, 197–217.
23. Antonsen, T. M.; Taguchi, T.; Gupta, A.; Palastro, J.; Milchberg, H. M. Resonant Heating of a Cluster Plasma by Intense Laser Light. *Phys. Plasmas* **2005**, *12*, 056703.
24. Lezius, M.; Dobosz, S. Hot Nanoplasmas from Intense Laser Irradiation of Argon Clusters. *J. Phys. B* **1997**, *30*, L251–L258.
25. Döppner, T.; Müller, J. P.; Przystawik, A.; Göde, S.; Tiggesbäumker, J.; Meiwes-Broer, K.-H.; Varin, C.; Ramunno, L.; Brabec, T.; Fennel, T. Steplike Intensity Threshold Behavior of Extreme Ionization in Laser-Driven Xenon Clusters. *Phys. Rev. Lett.* **2010**, *105*, 053401.
26. Ammosov, M. V.; Delone, N. B.; Krainov, V. P. Tunnel Ionization of Complex Atoms and of Atomic Ions in an Alternating Electromagnetic Field. *Sov. Phys. JETP* **1986**, *64*, 1191–1194.
27. Barnes, W.; Dereux, A.; Ebbesen, T. Surface Plasmon Subwavelength Optics. *Nature* **2003**, *424*, 824–830.
28. Boulais, E.; Robitaille, A.; Desjeans-Gauthier, P.; Meunier, M. Role of near-Field Enhancement in Plasmonic Laser Nanoablation Using Gold Nanorods on a Silicon Substrate: Comment. *Opt. Express* **2011**, *19*, 22556–22571.
29. Chen, Z.; Taflove, A.; Backman, V. Photonic Nanojet Enhancement of Backscattering of Light by Nanoparticles: A Potential Novel Visible-Light Ultramicroscopy Technique. *Opt. Express* **2004**, *12*, 1214–1220.
30. Ju, D.; Pei, H.; Jiang, Y.; Sun, X. Controllable and Enhanced Nanojet Effects Excited by Surface Plasmon Polariton. *Appl. Phys. Lett.* **2013**, *102*, 171109.
31. Ferrand, P.; Devilez, A.; Pianta, M.; Stout, B.; Bonod, N.; Popov, E.; Rigneault, H. Direct Imaging of Photonic Nanojets. *Opt. Express* **2008**, *16*, 209–215.
32. Guo, H.; Han, Y.; Weng, X.; Zhao, Y.; Sui, G.; Wang, Y.; Zhuang, S. Near-Field Focusing of the Dielectric Microsphere with Wavelength Scale Radius. *Opt. Express* **2013**, *21*, 2434–2443.
33. Grubisic, A.; Ringe, E.; Cobley, C. M.; Xia, Y.; Marks, L. D.; Van Duyne, R. P.; Nesbitt, D. J. Plasmonic near-Electric Field Enhancement Effects in Ultrafast Photoelectron Emission: Correlated Spatial and Laser Polarization Microscopy Studies of Individual Ag Nanocubes. *Nano Lett.* **2012**, *12*, 4823–4829.
34. Das, P.; Chini, T. K. Spectroscopy and Imaging of Plasmonic Modes over a Single Decahedron Gold Nanoparticle: A Combined Experimental and Numerical Study. *J. Phys. Chem. C* **2012**, *116*, 25969–25976.
35. Blackie, E. J.; Le Ru, E. C.; Etchegoin, P. G. Single-Molecule Surface-Enhanced Raman Spectroscopy of Nonresonant Molecules. *J. Am. Chem. Soc.* **2009**, *131*, 14466–14472.
36. Lahiri, B.; Holland, G.; Aksyuk, V.; Centrone, A. Nanoscale Imaging of Plasmonic Hot Spots and Dark Modes with the Photothermal-Induced Resonance Technique. *Nano Lett.* **2013**, *13*, 3218–3224.
37. Lumerical Solutions, Inc. Http://www.lumerical.com/tcad-Products/fdtd/.
38. DeVore, J. R. Refractive Indices of Rutile and Sphalerite. *J. Opt. Soc. Am.* **1951**, *42*, 416–419.
39. *Handbook of Optics*, Vol. 4, 3rd ed.; McGraw-Hill, 2009.
40. Salabat, A.; Alinoori, M. Viscosity, Density, and Refractive Index of Poly(vinylpyrrolidone) + 1-Propanol and + 2-Propanol at 298.15 K. *J. Chem. Eng. Data* **2009**, *54*, 1073–1075.
41. Palik, E. D. *Handbook of Optical Constants of Solids*; Academic Press: Boston, 1985.